Catal Lett (2012) 142:838–844
DOI 10.1007/s10562-012-0837-x

The Effect of Tin–Support Interaction on Catalytic Stability over Pt–Sn/*x*Al–SBA-15 Catalysts for Propane Dehydrogenation

Bao Khanh Vu · Eun Woo Shin · In Young Ahn · Jeong-Myeong Ha · Dong Jin Suh · Won-Il Kim · Hyoung-Lim Koh · Young Gyo Choi · Seung-Bum Lee

Received: 2 March 2012 / Accepted: 24 April 2012 / Published online: 12 May 2012

Abstract We prepared Pt–Sn/*x*Al–SBA-15 catalysts with various ratios of Al to Si and investigated them for propane dehydrogenation in order to understand the influence of the interaction between tin and the supports on catalytic stability. The weaker interaction between SnO_x and the supports leads to easier formation of Pt–Sn alloys. The formation of Pt–Sn alloys increases the stability of catalysts, and the stability of Pt–Sn/*x*Al–SBA-15 catalysts is inversely proportional to the aluminum content in SBA-15.

Keywords Dehydrogenation · Deactivation · Metal–support interaction

1 Introduction

The primary production method of propylene in the petrochemical industry is naphtha cracking, where ethylene is co-produced. Demand for propylene world-wide is growing faster than that of ethylene, which causes a shortfall in propylene supply from steam cracking. As a result, propane dehydrogenation has been considered to address the propylene shortfall. The addition of tin to Pt/support catalyst systems has been widely studied in the dehydrogenation of paraffins and has had a positive effect on the stability and selectivity to olefins. However, the stability of Pt–Sn supported catalysts is still unsatisfactory. The role of tin is to promote the mobility of coke precursors from metal to support, although it is not obvious how this is accomplished. Tin does not diminish the coke amount, but quite the opposite; however, the carbon formed is less inimical to activity because much of it is located on the support [1]. Various commercial catalysts have been developed for propane dehydrogenation: chromia-alumina (ABB Lummus Global), Pt/alumina with alkali, Cu, and Zn used as promoters (UOP LLC), and Pt/zinc aluminate with Sn used as a promoter (Phillips Petroleum) [2]. Although many efforts have been made to modify supported Pt catalysts, deactivation due to coking is still not completely overcome, and catalysts must undergo continuous or frequent regeneration processes to restore the catalytic activity promoters [3–9].

Many studies have used SBA-15 as a support for active CrO_x and VO_x species in oxidative propane dehydrogenation since SBA-15 possesses a high surface area and thermal and hydrothermal stability [10–17]. It was found that these materials show excellent catalytic performance. However, less attention has been paid to using SBA-15 as a support in propane dehydrogenation using Pt and Sn as an active site and a promoter, respectively. Recently, it has been reported that, over a SBA-15 support, smaller Pt particles are much more active and less selective than larger ones. Therefore, coking is significantly more successful in the former than that in the latter. Moreover, Pt–Sn/SBA-15 was revealed to have a higher activity and

B. K. Vu · E. W. Shin (✉)
School of Chemical Engineering and Bioengineering, University of Ulsan, Daehakro 102, Nam-gu, Ulsan 680-749, South Korea
e-mail: ewshin@mail.ulsan.ac.kr

I. Y. Ahn · J.-M. Ha · D. J. Suh
Korea Institute of Science and Technology, Wolsong-gil 5, Seongbuk-gu, Seoul 136-791, South Korea

W.-I. Kim · H.-L. Koh · Y. G. Choi
Production R&D Center, Hyosung Co., Hogye-dong, Dongan-gu, Anyang, Gyeounggi 431-080, South Korea

S.-B. Lee
Department of Chemical Engineering, Dankook University, Gyeonggi 448-701, South Korea

be more stable than Pt/SBA-15 due to higher Pt dispersion by Pt–Sn alloy formation (detected by energy dispersive X-ray spectroscopy) in Pt–Sn/SBA-15 catalysts. These have been explained by the different surface site heterogeneity values due to the difference in Pt particle size and the role of Sn in preferential coverage of these highly energetic Pt sites [18, 19]. Propane dehydrogenation over a Pt–Sn catalyst supported on alumina-modified SBA-15 exhibits greater activity than that on SBA-15 and has higher stability than that on γ-Al_2O_3. In addition, temperature-programmed reduction of tin species make it easy to reduce tin to its metallic state due to the weak interaction of Sn species with the SBA-15 support [20]. It is noteworthy that the reduction temperature in the reaction test of this study is lower than that of tin species and possibly lower than that of Pt–Sn alloy formation based on temperature-programmed reduction. Consequently, more characterization techniques should be involved in understanding the ability of Pt–Sn systems to correlate activity and stability.

The aim of this study is to investigate propane dehydrogenation over Pt–Sn/*x*Al–SBA-15 catalysts with various ratios of Al to Si. Particular emphasis will be placed on the Sn species-support interaction related to Pt–Sn alloy formation and therefore catalytic performance. To this end, catalysts were characterized by N_2 sorption, thermogravimetric analysis, powder X-ray diffraction, infrared Fourier spectroscopy, and X-ray photoelectron spectroscopy (XPS). In addition, catalytic performances were monitored by propane dehydrogenation in a microreactor.

2 Experimental

2.1 Catalyst Preparation

SBA-15 support was synthesized using triblock copolymer (Pluronic P123) as a template and tetraethyl orthosilicate as a silica source at room temperature, according to the procedure reported in the literature [21, 22]. Al-impregnation was conducted by the excess aqueous solution technique. A predetermined amount of aluminum nitrate nonahydrate ($Al(NO_3)_3{\cdot}9H_2O$, Sigma-Aldrich, 99.997 %) was dissolved in 100 ml of deionized water, and then 5.0 g of SBA-15 was soaked in the prepared solution. After that, the mixture was sonicated for 10 min and heated at 60 °C with stirring until a dry powder was obtained. The final powder was dried at 100 °C for 12 h before calcination at 600 °C for 6 h. Aluminum was incorporated into SBA-15 with three atomic ratios of Si to Al (10, 20, and 40).

A total of 2.0 wt% of each metal (Pt and Sn) was loaded onto supports using an incipient wetness impregnation technique. $H_2PtCl_6{\cdot}6H_2O$ (Sigma-Aldrich, ≥37.5 % Pt basis) and $SnCl_2{\cdot}2H_2O$ (Sigma-Aldrich, ≥98 %) precursors were dissolved in a predetermined amount of deionized water. One aliquot containing 200 µl precursor was evenly dispersed over the calcined supports. This procedure was repeated until the ratio of liquid to support was 1.0 ml/g. Catalysts were dried at room temperature for 24 h at 100 °C for 12 h in an oven and calcined at 600 °C for 6 h in a furnace. The catalysts were labeled as Pt–Sn/*x*Al–SBA-15, in which *x* is the molar ratio of Al to Si.

2.2 Characterization

The surface areas and pore size distributions of the catalysts were characterized by a nitrogen sorption technique (Micromeritics ASAP 2020, USA). Samples were degassed under a vacuum at 300 °C for 4 h prior to automatic analyzer analysis at −196.15 °C. Coke content was determined by a thermogravimetric analyzer (TA Instruments Q50, USA). Approximately 10 mg of spent catalyst was charged into the sample pan and heated to 800 °C at a rate of 20 °C/min in flowing air.

Small and wide angle X-ray diffraction (XRD) patterns were obtained on a Rigaku D/MAX-2200 powder X-ray diffractometer (Rigaku Corporation, Japan) using a Cu Kα radiation source ($\lambda = 0.15418$ nm). Fourier transform infrared spectra (FT-IR) of the samples in the form of KBr powder-pressed pellets were measured on a Nicolet 380 FT-IR spectrophotometer (USA) under ambient conditions. An XPS study of catalysts was conducted using a Thermo VG Scientific ESCALAB-250 instrument (USA) with an excitation source of Al Kα radiation. In addition to a binding energy scan range from 0 to 1,200 eV for the identification of all detectable elements, detailed scans for the chemical state identification and quantification were obtained.

2.3 Reaction Test

Propane dehydrogenation was performed in a fixed-bed reactor at 1 bar and 600 °C. The catalyst (150 mg) was reduced in situ in pure H_2 (50 ml/min) at 600 °C for 3 h and then purged by N_2 (100 ml/min) for 10 min to remove the remaining H_2. Then, the reaction mixture consisting of N_2 (50 ml/min) and C_3H_8 (15 ml/min) was fed into the reactor. The product was sampled through a six-port valve via a sample loop (0.25 ml) into a gas chromatograph (YOUNG LIN-Acme 6000 GC, South Korea) equipped with an FID detector and a 30 m × 0.53 mm HP-PLOT Al_2O_3 "KCl" capillary column.

3 Results and Discussion

The isotherms and pore size distributions of the reduced catalysts were characterized by N_2 sorption and are shown

in Fig. 1, and the textural properties are listed in Table 1. Decreases in the total surface area and pore volume were attributed to both plugging of micropores and coating of the mesopores by alumina. The data in Table 1 show that alumina mainly filled the micropores because the incorporation of Al to SBA-15 resulted in a loss of micropore volume in the SBA-15. In contrast, the pore size of SBA-15 remained unchanged.

Figure 2 shows the FT-IR spectra of the supports. In the spectrum of the SBA-15 sample, three well-resolved bands at 458, 800, and 1080 cm^{-1} correspond to rocking, bending, and asymmetric stretching of the intertetrahedral oxygen atoms in the SiO_2 structure, respectively [22]. It is noteworthy that the intensity of the band at 965 cm^{-1} assigned to the Si–(OH) stretching mode decreased proportionally as the aluminum content increased. This observation can be explained by the interaction between the silanol groups on the SBA-15 surface and the impregnated-Al component via the condensation process. The consumption of silanol groups on the SBA-15 surface results in attenuation of the intensity of the band at 965 cm^{-1}. Thus, the impregnated-Al component was not inserted into the SBA-15 framework since the intensities of the bands (458, 800, and 1080 cm^{-1}) representing the SiO_2 structure remain unchanged among the samples.

The small-angle XRD pattern of the reduced Pt–Sn/SBA-15 catalyst, in Fig. 3, shows three well-resolved peaks at 0.9°, 1.6°, and 1.8° corresponding to (100), (110), and (200) reflections, respectively. These reflections present a 2D

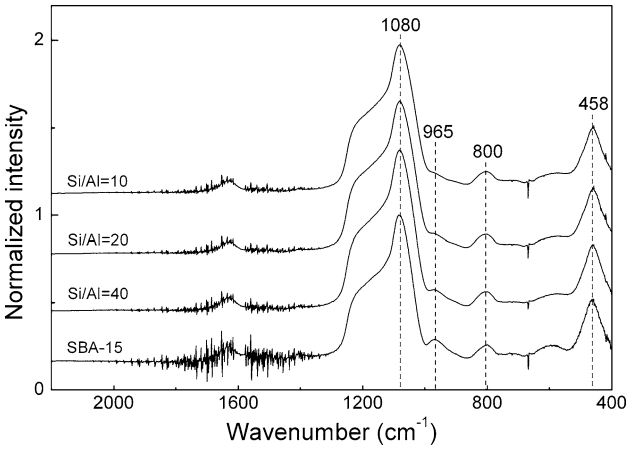

Fig. 2 FT-IR of the *x*Al–SBA-15 supports

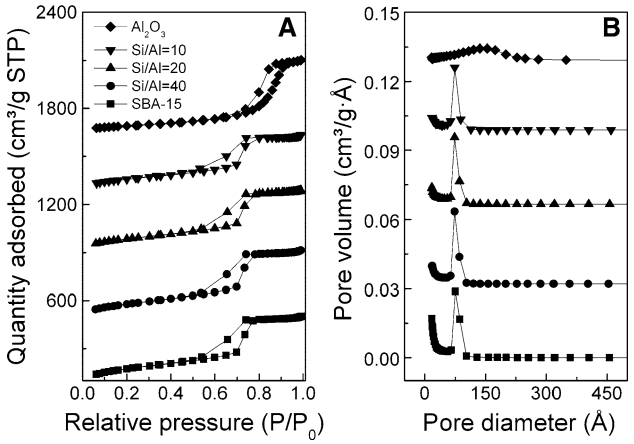

Fig. 1 N_2 adsorption–desorption measurements of **a** isotherms, and **b** pore size distributions of the reduced Pt–Sn/*x*Al–SBA-15 catalysts

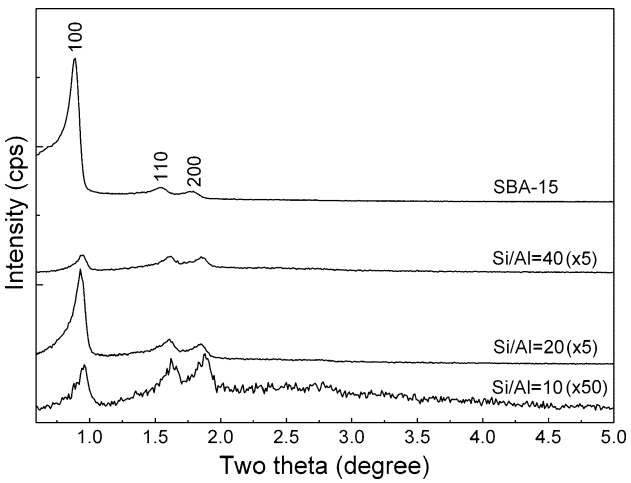

Fig. 3 Small-angle X-ray diffraction patterns of the reduced Pt–Sn/*x*Al–SBA-15 catalysts

Table 1 Pore structure parameters of samples calculated from the desorption branch of the nitrogen sorption isotherm using the Barret-Joyner-Halenda formula

Reduced Pt–Sn/*x*Al–SBA-15	BET surface area (m^2/g)	Micropore surface area (m^2/g)	Pore diameter (nm)	Pore volume (cm^3/g)	Micropore volume (cm^3/g)
SBA-15	589	210	5.6	0.80	0.105
Si/Al = 40	522	142	5.6	0.73	0.058
Si/Al = 20	437	97	5.6	0.66	0.047
Si/Al = 10	392	86	5.5	0.60	0.041
Al_2O_3	212	9.2	9.4	0.74	0.004

hexagonally symmetric pore structure with a space group of *p6mm*. For Al-modified SBA-15 samples, there is a decrease in the overall diffraction intensities, which is probably due to different scattering properties of alumina [23]. However, the small angle XRD patterns of the Al-modified SBA-15 samples demonstrate that the hexagonally ordered pore structure of SBA-15 was observed during all processes including the increased Al content, loading Pt and Sn, calcination, and reduction. The expansion in the unit cell with increasing aluminum content, which is a rule in zeolite chemistry, is caused by the Al–O bond being longer (1.75 Å) than the Si–O bond (1.60 Å) [24]. However, in our XRD patterns, all peak positions of the Al-modified SBA-15 samples were shifted to have a smaller unit cell, which can be explained by the fact that the impregnated-Al component was not inserted into the SBA-15 framework, as evidenced by the FT-IR results. The interaction between the silanol groups on the SBA-15 surface and impregnated-Al components via condensation reaction probably leads to the contraction of the unit cell of SBA-15. A previous work revealed that the contraction of a unit cell is caused by the condensation of Si–(OH) units in the channel wall of MCM-41 [25]. However, this contraction of the unit cell with increased aluminum content was suggested to be due to the substitution of silicon by aluminum [26].

To reveal the formation of metallic phases over calcined and reduced catalysts, wide angle XRD was recorded, and the patterns are presented in Fig. 4. The formation of Pt (PDF No.: 00-004-0802) and SnO_2 phases (PDF No.: 00-041-1445) were observed over the calcined Pt–Sn/*x*Al–SBA-15 catalysts, while only a Pt phase was detected over the calcined Pt–Sn/Al_2O_3 catalyst. This indicates that a strong interaction between Sn species and Al_2O_3 leads to high dispersion of SnO_x, and therefore no SnO_x phase can be detected. Upon reduction in H_2, the SnO_2 phase over the calcined Pt–Sn/*x*Al–SBA-15 catalysts was partially reduced to Sn in the metallic state, and then the metallic Sn combined with Pt to form Pt–Sn alloy (AMCSD No.: 99-101-0506) and Pt_3–Sn alloy (PDF No.: 00-035-1360). However, in the reduced Pt–Sn/Al_2O_3 sample, no Pt–Sn alloy formation was observed due to a strong interaction between SnO_x and Al_2O_3, which hinders the reducibility of SnO_x to metallic Sn. This observation opposes our previous finding that there are two types of Pt–Sn alloys formed over an Al_2O_3 support after reduction [27]. This difference can be explained by the fact that the Sn content is an important factor contributing to reducibility. Higher Sn content in our previous study (3 wt%) probably resulted in easier reducibility and therefore lead to more ready formation of Pt–Sn alloys. In addition to the effect of supports on the formation of Pt–Sn alloys, the use of platinum and tin precursors had important impact on the feasibility of formation of Pt–Sn phases. The bimetallic precursor, $[Pt(NH_3)_4][SnCl_6]$ led to sample showing more Pt–Sn alloys than sample obtained

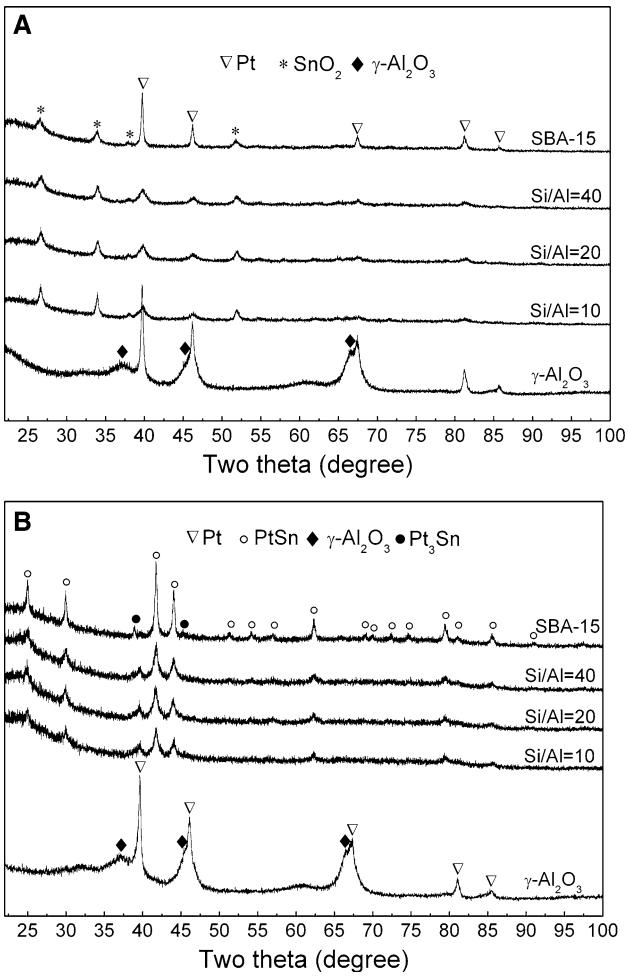

Fig. 4 Wide-angle X-ray diffraction patterns of **a** the calcined and **b** the reduced Pt–Sn/*x*Al–SBA-15 catalysts

from conventional coimpregnation of H_2PtCl_6 and $SnCl_4$ [28]. On the contrary to our observation, this finding also showed that coimpregnation of H_2PtCl_6 and $SnCl_2$ with 1.5 wt% Pt and 1.5 wt% Sn on Al_2O_3 resulted in a small portion of Pt–Sn alloys in the reduced catalyst. Therefore, the formation of Pt–Sn alloys should be dependent on route of treatment of catalysts during preparation as well. The crystallite sizes of SnO_2 and the metallic phases were calculated using the Scherrer equation and are listed in Table 2. Crystallite size data show that the combination of Al_2O_3 and SBA-15 results in smaller metallic phase size. This fact can be connected to the combination of a higher surface area of SBA-15 versus Al_2O_3 and a higher value of the point of zero charge in Al_2O_3 versus SBA-15. In other words, the impregnated-Al component probably formed a thin layer of Al_2O_3 on the wall of SBA-15 via condensation. This combination results in the attenuation of intensity of the 960 cm^{-1} band as observed by FT-IR and smaller sizes of the metallic phases, as evidenced by XRD.

Table 2 Crystallite sizes obtained by the Scherrer equation (profile fitting with pseudo-Voigt)

Pt–Sn/*x*Al–SBA-15 catalyst	Calcined		Reduced	
	Pt	SnO_2	Pt–Sn	Pt
SBA-15	27.9	12.3	32.0	nd
Si/Al = 40	8.7	11.5	19.7	nd
Si/Al = 20	8.5	11.5	16.4	nd
Si/Al = 10	8.9	16.4	18.4	nd
Al_2O_3	29.4	nd	nd	26.0

nd not detected

XPS spectra of the Sn 3d level of the calcined and reduced catalysts were measured and are presented in Fig. 5. The binding energies (BEs) and full widths at half maximum (FWHMs) of Pt 4f7/2 and Sn 3d5/2 are summarized in Table 3. The BEs of the Pt 4f7/2 level of the calcined catalysts ranged from 70.56 to 71.92 eV, indicating that the Pt phase was in the metallic state over the calcined catalysts. This observation is consistent with the XRD data discussed above that showed the Pt phase identified by a characteristic peak of (111) reflection over the calcined catalysts. After reduction, it is notable that the BEs and FWHMs of Pt 4f7/2 of the reduced catalysts are similar to those of the calcined catalysts. This indicates that the Pt phase was in the active state over the calcined catalysts.

More interestingly, the BEs and FWHMs of Sn 3d5/2 showed pronounced differences between the calcined and reduced catalysts. Upon reducing, the BEs of Sn 3d5/2 of the reduced catalysts shifted slightly to lower values, and the FWHMs were significantly broader than the calcined catalysts. However, over Pt–Sn/Al_2O_3 catalyst, the FWHMs of the calcined and reduced catalysts exhibited similar values. This observation implies that the reducibility of SnO_x species to metallic Sn over pure silica or Al-modified silica supports is easier than that over alumina support. In other words, the stronger SnO_x-support interaction leads to increased difficulty in the reduction of SnO_x to metallic Sn, therefore inhibiting the formation of Pt–Sn alloys. XPS findings agreed with XRD data that show Pt–Sn alloys over SBA-15 or Al-modified SBA-15 supports but not over Al_2O_3.

Catalytic performances of the supported Pt–Sn catalysts during propane dehydrogenation are shown in Fig. 6a. To compare the deactivation rates among catalysts, we defined the deactivation parameter as follows: $D = (X_0 - X_f) \times 100/X_0$, where X_0 and X_f are the initial and final propane conversion, respectively. The normalized conversions are also demonstrated in Fig. 6b for comparing the deactivation of catalyst versus time on stream. From the normalized propane conversion versus time on stream and the data in Table 4, it can be seen that the catalyst deactivation rate increased with increased aluminum content. The support having higher aluminum content resulted in faster deactivation rate. This trend of deactivation with increased aluminum content can be explained by the different extents of formation of Pt–Sn alloys on different catalysts, as observed by XRD. In other words, the weaker SnO_x-support interaction lead to easier formation of Pt–Sn alloys; therefore, the stability of the catalysts was improved.

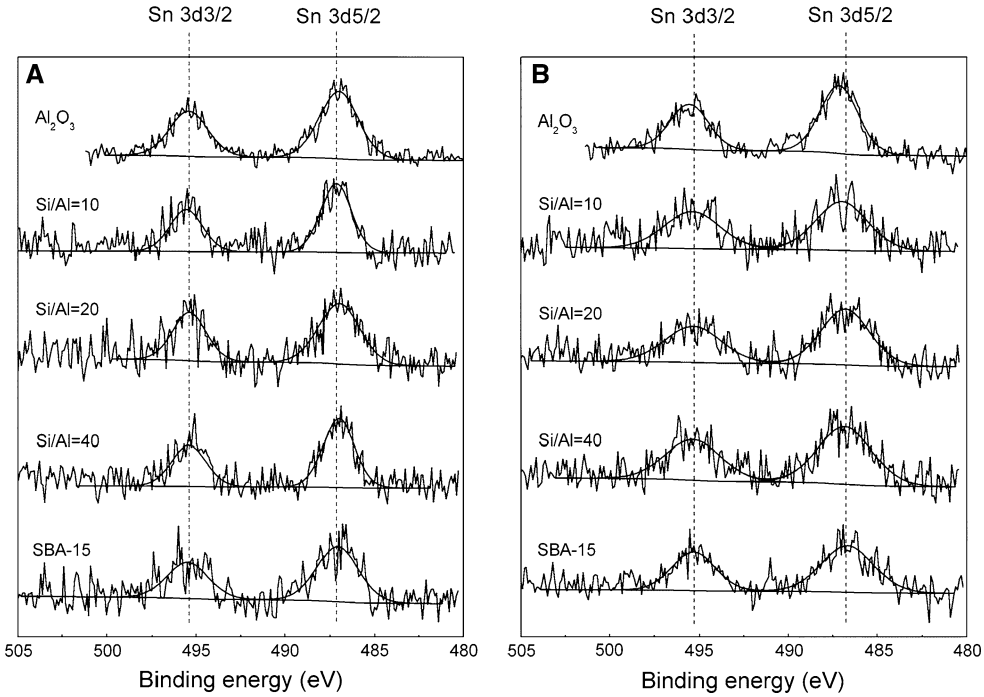

Fig. 5 X-ray photoelectron spectra of the Sn 3d level of **a** the calcined and **b** the reduced Pt–Sn/*x*Al–SBA-15 catalysts

Table 3 BEs and FWHMs of Pt 4f7/2 and Sn 3d5/2 obtained by XPS from the calcined and reduced samples

Pt–Sn/*x*Al–SBA-15 catalyst	Calcined				Reduced			
	Pt 4f7/2		Sn 3d5/2		Pt 4f7/2		Sn 3d5/2	
	BE	FWHM	BE	FWHM	BE	FWHM	BE	FWHM
SBA-15	71.56	2.4	487.07	2.7	71.44	2.4	486.76	3.3
Si/Al = 40	71.92	3.0	487.01	2.1	71.99	2.8	486.84	3.4
Si/Al = 20	71.72	2.6	486.91	2.7	71.72	2.6	486.81	3.3
Si/Al = 10	71.69	2.7	487.12	2.0	71.84	2.8	487.02	3.6
Al_2O_3	–	–	487.05	2.4	–	–	487.14	2.5

– Pt 4f totally overlapped with Al 2p

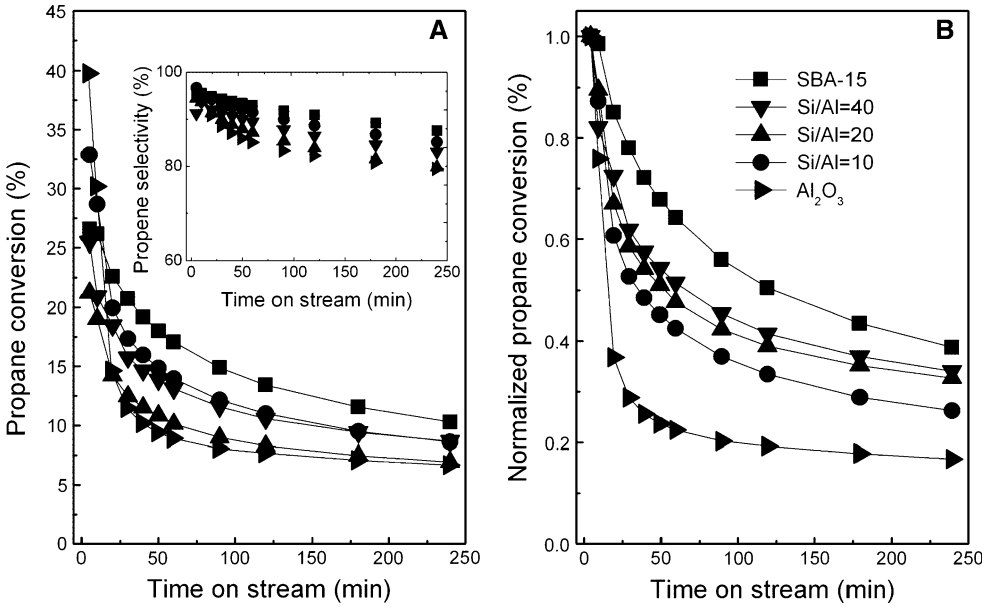

Fig. 6 Catalytic performances of **a** propane conversion and propene selectivity versus time on stream and **b** normalized propane conversion versus time on stream

Apparently, the deactivation of the catalysts can be correlated with the coke content listed in Table 4. The catalyst with higher aluminum content in the support produced higher coke amount as measured by TGA since the acidic sites on alumina could catalyze the coke formation [29]. However, in our previous study, we found that that the coke content was not a main factor in determination of catalytic deactivation. In that study, we prepared two catalysts, Pt/Al_2O_3 and Pt/SBA-15 with similar Pt loadings, and found that the coke content on spent Pt/Al_2O_3 catalyst was two times higher than that on spent Pt/SBA-15 catalyst; however, the deactivation rates of the two catalysts were almost equal [30]. Huang et al. [20] investigated propane dehydrogenation over the Pt–Sn catalyst supported on alumina-modified SBA-15 and revealed that the Pt–Sn/Al_2O_3/SBA-15 catalyst has a larger bare fraction of Pt surface after coke deposition, leading to higher catalytic stability compared to that of the Pt–Sn/Al_2O_3 catalyst. Through temperature-programmed reduction, Huang et al. have shown that, on pure siliceous SBA-15, the dispersed tin oxides are easier to reduce to a metallic state, and metallic tin possibly forms alloys with Pt. However, the interaction between tin oxides and support becomes stronger after modification of SBA-15 by Al_2O_3; therefore, tin oxides are more difficult to reduce to metallic tin. In our experiment with high Pt and Sn contents, the formation of Pt–Sn alloys on SBA-15 and *x*Al–SBA-15 supports was observed clearly by XRD. These Pt–Sn alloys enhance the catalytic stability, and the role of Pt–Sn alloys in stabilizing the catalysts is usually explained by the geometric and electronic effects of Sn on Pt sites. The geometric effect of Sn is to dilute and reduce the number of adjacent Pt atoms; this dilution of Pt by Sn inhibits the coke formation that requires a large ensemble of Pt atoms [31]. The electronic effect of Sn is to change the electron density of Pt atoms; this decreases the bonding strength between Pt atoms and coke precursors and therefore keeps the Pt surface clean [32].

Table 4 Deactivation parameters and coke content

Spent Pt–Sn/*x*Al–SBA-15 catalyst	X_0^a (%)	X_f^b (%)	D[c]	Coke[d] (wt%)
SBA-15	26.5	10.3	61.1	nd
Si/Al = 40	25.5	8.7	65.9	0.4
Si/Al = 20	21.2	6.9	67.5	0.8
Si/Al = 10	32.9	8.6	73.9	1.7
Al_2O_3	39.8	6.7	83.2	5.3

nd not detected

[a] Initial conversion

[b] Final conversion

[c] Deactivation parameter

[d] Obtained from TGA

4 Conclusions

The stability of Pt–Sn/*x*Al–SBA-15 catalysts is inversely proportional to the aluminum content in the SBA-15 support. The role of Sn as a promoter in the supported Pt–Sn catalysts can be enhanced by the weak interaction between SnO_x species and supports. Weaker interactions between SnO_x species and supports result in easy formation of Pt–Sn alloys, which are necessary for high catalyst stability.

Acknowledgments This work was supported by a grant from the Energy Efficiency & Resources Program of the Korea Institute of Energy Technology Evaluation and Planning (KETEP) funded by the Ministry of Knowledge Economy of the Korean government (No. 2007MCC24P0230202009).

References

1. Bond BC (2005) Metal-catalysed reactions of hydrocarbons. Kluwer/Plenum, New York
2. Rase HF (2000) Handbook of commercial catalysts: heterogeneous catalysts, 1st edn. CRC Press, Austin
3. Yu C, Ge Q, Xu H, Li W (2006) Appl Catal A Gen 315:58
4. Del Angel G, Bonilla A, Peña Y, Navarrete J, Fierro JLG, Acosta DR (2003) J Catal 219:63
5. Casella ML, Siri GJ, Santori GF, Ferretti OA, Ramirez-Corredores MM (2000) Langmuir 16:5639
6. Yu C, Xu H, Ge Q, Li W (2007) J Mol Catal A Chem 266:80
7. Siri GJ, Bertolini GR, Casella ML, Ferretti OA (2005) Mater Lett 59:2319
8. Bocanegra SA, Guerrero-Ruiz A, de Miguel SR, Scelza OA (2004) Appl Catal A Gen 277:11
9. Bosch P, Valenzuela MA, Zapata B, Acosta D, Aguilar-Ríos G, Maldonado C, Schifter I (1994) J Mol Catal 93:67
10. Liu YM, Cao Y, Yi N, Feng WL, Dai WL, Yan SR, He HY, Fan KN (2004) J Catal 224:417
11. Gruene P, Wolfram T, Pelzer K, Schlögl R, Trunschke A (2010) Catal Today 157:137
12. Michorczyk P, Ogonowski J, Niemczyk M (2010) Appl Catal A Gen 374:142
13. Xu J, Chen M, Liu YM, Cao Y, He HY, Fan KN (2009) Microporous Mesoporous Mater 118:354
14. Michorczyk P, Ogonowski J, Zeńczak K (2011) J Mol Catal A Chem 349:1
15. Liu YM, Cao Y, Zhu KK, Yan SR, Dai WN, He HY, Fan KN (2002) Chem Commun 23:2832
16. Zhang X, Yue Y, Gao Z (2002) Catal Lett 83:19
17. Aktas O, Yasyerli S, Dogu G, Dogu T (2010) India Eng Chem Res 49:6790
18. Kumar MS, Chen D, Walmsley JC, Holmen A (2008) Catal Commun 9:747
19. Kumar MS, Chen D, Holmen A, Walmsley JC (2009) Catal Today 142:17
20. Huang L, Xu B, Yang L, Fan Y (2008) Catal Commun 9:2593
21. Zhao D, Feng J, Huo Q, Melosh N, Fredrickson GH, Chmelka BF, Stucky GD (1998) Science 279:548
22. Shin EW, Han JS, Jang M, Min SH, Park JK, Rowell RM (2003) Environ Sci Technol 38:912
23. Cónsul JMD, Peralta CA, Benvenutti EV, Ruiz JAC, Pastore HO, Baibich IM (2006) J Mol Catal A Chem 246:33
24. Borade RB, Clearfield A (1997) Catal Lett 31:267
25. Cheng CF, Park DH, Klinowski J (1997) J Chem Soc. Faraday Trans 93:193
26. Romero AA, Alba MD, Klinowski J (1998) J Phys Chem B 102:123
27. Vu BK, Song MB, Ahn IY, Suh YW, Suh DJ, Kim WI, Koh HL, Choi YG, Shin EW (2011) Appl Catal A Gen 400:25
28. Kappenstein C, Guérin M, Lázár K, Matusek K, Paál Z (1998) J Chem Soc. Faraday Trans 94:2463
29. Li Q, Sui Z, Zhou X, Zhu Y, Zhou J, Chen D (2011) Top Catal 54:888
30. Vu BK, Bok S, Ahn IY, Shin EW (2009) Catal Lett 133:376
31. Bastein AGTM, Toolenaar FJCM, Ponec V (1984) J Catal 90:88
32. Burch R (1981) J Catal 71:348